Sensing and Imaging (2018) 19:31
https://doi.org/10.1007/s11220-018-0215-x

ORIGINAL PAPER

Dynamic Analysis of Rectangular Micro-plates Under Mechanical Shock in Presence of Electrostatic Actuation

Amir R. Askari[1] · **Masoud Tahani**[2]

Received: 28 March 2018 / Revised: 23 June 2018

Abstract

Besides one dimensional beam-type MEMS, two dimensional electrically actuated rectangular micro-plates have lots of applications in micro-engineering. However, there exist only a few works devoted to the analysis of such structures in the open literature to date. Therefore, the present work focuses on the dynamic behavior of electrically actuated rectangular micro-plates under mechanical shock. The micro-plate is modeled using the non-linear Kirchhoff plate theory and the shock is assumed to be induced according to the base excitation scheme. The micro-plate motion is simulated through a novel and computationally very efficient reduced order model which accounts for the inherent non-linearity of distributed electrostatic pressure and the geometric non-linearity of von Kármán mid-plane stretching as well as the influences of both in-plane and out-of-plane displacements. The present findings are compared and successfully validated by those obtained through three-dimensional finite element analysis carried out in COMSOL Multiphysics commercial software as well as the available static results in the literature. It is found that the present procedure can remove the long run-time limitation of the finite element method and produce robust results over the whole operation range of the device up to its instability threshold especially for systems subjected to enormous shock accelerations.

Keywords Micro-electro-mechanical plates · Reduced order model · Dynamic pull-in instability · Mechanical shock

✉ Amir R. Askari
amaskari@gmail.com; ar.askari@hsu.ac.ir

[1] Department of Mechanical Engineering, Hakim Sabzevari University, Sabzevar, Iran

[2] Department of Mechanical Engineering, Ferdowsi University of Mashhad, Mashhad, Iran

Published online: 01 August 2018

1 Introduction

Analyzing the mechanical behavior of electrically actuated micro-structures, which can be considered as the building blocks of micro-electro-mechanical systems (MEMS) [1], is so necessary nowadays. In general, an electrically actuated micro-structure is a conductive and elastic thin plate suspended over a stationary rigid electrode and deflects toward its substrate by applying an external voltage [2]. One of the most important phenomena associated with such systems is pull-in instability which occurs when the input voltage exceeds a critical value called pull-in voltage. In some sorts of MEMS devices such as resonant micro-sensors, pull-in instability can be treated as a source of failure [3]. Therefore, such systems are designed far from this instability. It is noteworthy that some other types of micro-systems such as capacitive micro-switches work based on pull–in instability [4]. Hence, pull–in instability is desirable in these systems and they are designed to pull–in at a certain value of input voltage. Therefore, it can be concluded that regardless the type and application of a micro-device, it is so essential to determine its instability threshold accurately.

MEMS devices are usually faced with some environmental forces such as mechanical shock which highly affects their motion. Mechanical shock can induce high dynamic loads on micro-structures and cause the structure to hit the stationary electrode underneath it [5–7]. This fact can be desirable in some cases such as sensors of vehicle airbags and employed as the basis of the sensing method [5]. Also, it can be undesirable in some other cases such as micro-switches and makes the electrodes to stick each other at a voltage much lower than the one predicted, considering the effect of electrostatic actuation alone [5]. Since the majority of micro-structures are fabricated from silicon or polysilicon, which are very tough against bending stresses induced from shock acceleration, failure in MEMS unlike in large-scale devices does not due to high stresses [5–7]. The most important source of failure in MEMS is stiction and electric short circuits; however, the incidents between a movable part and other parts or a substrate may lead to failure due to the severe contact stresses [5–7]. It is worth noting that although lots of research efforts have been devoted to the analysis of micro-structures under shock pulse acceleration to date [8–11]; there exist only a few studies in the literature which investigated the response of micro-structures subjected to combined actions of electrostatic actuation and mechanical shock. Therefore, to find the design parameters of MEMS devices, analyzing the response of micro-systems under combined effect of these two excitations is so essential.

Due to the coupling between electrical and structural physics as well as the strong non-linearities arising in the field of electrically actuated micro-structures especially those subjected to mechanical shock acceleration, modelling of these systems is very challenging [5–7, 12]. It is worth noting that although variety of mathematical procedures have been employed to investigate the mechanical behavior of MEMS structures to date [13–39], reduced order modelling, due to its lower run-time and the robustness in producing results over the whole operation range of the device, can be treated as an exclusive procedure in comparison to other ones [17]. In general, reduced order models

(ROMs) eliminate the spatial dependence in the governing partial differential equations (PDEs) of motion and perform a transformation from the physical coordinates of the device to a set of generalized coordinates. In this way, employing some usual mathematical techniques such as the Galerkin weighted residual method (GWRM), the governing PDEs of motion are reduced to a set of ordinary differential equations (ODEs) in time which can be solved much more easily than the governing equations themselves [17].

Due to the aforementioned desirable features of generating ROMs, employing this procedure have strongly been suggested for modelling electrically actuated microstructures especially those subjected to mechanical shock [5–7]. In this way, Younis and his co-workers [6, 7] presented a multi-mode ROM for beam-type MEMS with clamped–clamped and clamped-free boundary conditions. They compared and validated their findings with those obtained by three-dimensional (3-D) finite element (FE) simulation carried out in ANSYS commercial software. It is noteworthy that neither their FE nor multi-mode reduced order models could capture dynamic pull–in instability for cases subjected to enormous shock accelerations. For the purpose of removing this limitation, Askari and Tahani [5] presented an alternative ROM for the same problem. They showed that their alternative ROM, which had only one degree of freedom (DOF), enjoys from lower run-time and the capability of capturing pull–in instability in cases under enormous shock loads.

Unlike the numerous applications of plate-type MEMS, especially fully clamped ones [40], the majority of presented ROMs for MEMS devices are based on beam models and there exist only a few plate-based ROMs in the literature. Furthermore, due to the high complexity involved in the set of reduced ODEs extracted from the available plate-based ROMs [16, 17, 41], according to the best of authors' knowledge, the response of such systems under mechanical shock has not been investigated to date. To this end, an efficient ROM based on the geometric non-linear Kirchhoff's plate model is developed. The results of the present work are validated through direct comparison with those available in the literature. Furthermore, since there exist no published results in the open literature for electrically actuated micro-plates under mechanical shock, the present findings for such systems are verified by those obtained through 3-D FE simulation performed in COMSOL Multiphysics commercial software [42].

2 Problem Formulation

Consider an electrically actuated rectangular micro-plate with the density of ρ subjected to mechanical shock as it is shown in Fig. 1. According to this figure, the dimensions of the micro-plate are set to a, b and h. Moreover, the initial gap between the non-actuated micro-plate and the substrate is assumed to be d.

According to basic hypothesis of the Kirchhoff thin plate theory, the displacement field $\left(\hat{u}_1, \hat{u}_2, \hat{u}_3\right)$ of an arbitrary point on the micro-plate can be expressed as [43]

$$\hat{u}_1\left(\hat{x}, \hat{y}, \hat{z}, \hat{t}\right) = \hat{u}\left(\hat{x}, \hat{y}, \hat{t}\right) - \hat{z}\frac{\partial}{\partial \hat{x}}\hat{w}\left(\hat{x}, \hat{y}, \hat{t}\right) \tag{1a}$$

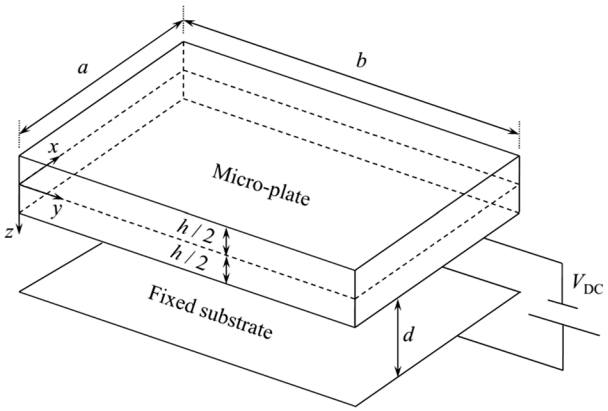

Fig. 1 Schematic of an electrically actuated micro-plate

$$\hat{u}_2(\hat{x},\hat{y},\hat{z},\hat{t}) = \hat{v}(\hat{x},\hat{y},\hat{t}) - \hat{z}\frac{\partial}{\partial\hat{y}}\hat{w}(\hat{x},\hat{y},\hat{t}) \tag{1b}$$

$$\hat{u}_3(\hat{x},\hat{y},\hat{z},\hat{t}) = \hat{w}(\hat{x},\hat{y},\hat{t}) \tag{1c}$$

where $\hat{u}$, $\hat{v}$ and $\hat{w}$ are the displacements of a point on the mid-plane of the micro-plate along the $\hat{x}$, $\hat{y}$ and $\hat{z}$ directions, respectively. For systems with small strains, moderate slopes and large deflections, as those occurred in MEMS applications [17], the strain-displacement relations can be approximated by the von Kármán theory [43]. Therefore, the non-zero strain components associated with the displacement field presented in Eq. (1) take the form

$$\varepsilon_{\hat{x}} = \hat{u}_{,\hat{x}} + \tfrac{1}{2}\hat{w}^2_{,\hat{x}} - \hat{z}\,\hat{w}_{,\hat{x}\hat{x}} \tag{2a}$$

$$\varepsilon_{\hat{y}} = \hat{v}_{,\hat{y}} + \tfrac{1}{2}\,\hat{w}^2_{,\hat{y}} - \,\hat{z}\,\hat{w}_{,\hat{y}\hat{y}} \tag{2b}$$

$$\gamma_{\hat{x}\hat{y}} = \hat{u}_{,\hat{y}} + \hat{v}_{,\hat{x}} + \hat{w}_{,\hat{x}}\hat{w}_{,\hat{y}} - 2\hat{z}\,\hat{w}_{,\hat{x}\hat{y}} \tag{2c}$$

where the comma sign followed by an independent variable refers to the partial derivative with respect to that variable. Employing the Hamilton principle [43], the governing equations of motion in terms of the micro-plate displacements after following some straightforward mathematical operations are given by [16, 43]

$$\hat{u}_{,\hat{x}\hat{x}} + \hat{w}_{,\hat{x}}\hat{w}_{,\hat{x}\hat{x}} + \frac{1-\nu}{2}\left(\hat{u}_{,\hat{y}\hat{y}} + \hat{w}_{,\hat{x}}\hat{w}_{,\hat{y}\hat{y}}\right) + \frac{1+\nu}{2}\left(\hat{v}_{,\hat{x}\hat{y}} + \hat{w}_{,\hat{y}}\hat{w}_{,\hat{x}\hat{y}}\right) = 0 \tag{3a}$$

$$\hat{v}_{,\hat{y}\hat{y}} + \hat{w}_{,\hat{y}}\hat{w}_{,\hat{y}\hat{y}} + \frac{1-\nu}{2}\left(\hat{v}_{,\hat{x}\hat{x}} + \hat{w}_{,\hat{y}}\hat{w}_{,\hat{x}\hat{x}}\right) + \frac{1+\nu}{2}\left(\hat{u}_{,\hat{x}\hat{y}} + \hat{w}_{,\hat{x}}\hat{w}_{,\hat{x}\hat{y}}\right) = 0 \tag{3b}$$

$$\frac{Eh}{1-\nu^2}\left[\hat{w}_{,\hat{x}\hat{x}}\left(\hat{u}_{,\hat{x}}+\frac{1}{2}\left(\hat{w}_{,\hat{x}}\right)^2+\nu\hat{v}_{,\hat{y}}+\frac{\nu}{2}\left(\hat{w}_{,\hat{y}}\right)^2\right)+(1-\nu)\hat{w}_{,\hat{x}\hat{y}}\left(\hat{u}_{,\hat{y}}+\hat{v}_{,\hat{x}}+\hat{w}_{,\hat{x}}\hat{w}_{,\hat{y}}\right)\right.$$
$$\left.+\hat{w}_{,\hat{y}\hat{y}}\left(\hat{v}_{,\hat{y}}+\frac{1}{2}\left(\hat{w}_{,\hat{y}}\right)^2+\nu\hat{u}_{,\hat{x}}+\frac{\nu}{2}\left(\hat{w}_{,\hat{x}}\right)^2\right)\right]+F_{\mathrm{es}}+F_{\mathrm{sh}}=\rho h\hat{w}_{,\hat{t}\hat{t}}+\frac{Eh^3}{12\left(1-\nu^2\right)}\nabla^4\hat{w} \tag{3c}$$

where E, ν, F_{es} and F_{sh}, respectively, refer to the Young Modulus, Poisson ratio, electrostatic attraction and shock pressure. In addition, the ∇^4 operator for a two-dimensional Cartesian space yields

$$\nabla^4=\left(\frac{\partial^4}{\partial\hat{x}^4}+2\frac{\partial^4}{\partial\hat{x}^2\partial\hat{y}^2}+\frac{\partial^4}{\partial\hat{y}^4}\right) \tag{4}$$

The electrostatic attraction per unit area of the micro-plate (i.e. F_{es}) also takes the form [16]

$$F_{es}=\frac{\varepsilon V_{\mathrm{DC}}^2}{2(d-w)^2} \tag{5}$$

where ε is the dielectric constant of the medium and V_{DC} is the external applied voltage. The shock pressure, which is transmitted to the micro-structure through its supports, can also be defined as [5]

$$F_{\mathrm{sh}}=F_0 g\left(\hat{t}\right) \tag{6}$$

where F_0 is the amplitude of the shock pressure and $g\left(\hat{t}\right)$ specifies its profile. According to the base excitation scheme [44], the shock pressure amplitude becomes

$$F_0=\rho h a_0 \tag{7}$$

in which a_0 is the amplitude of shock pulse acceleration. The shape of the actual shock pressures in most of the cases can successfully be approximated by the half-sin profile which can mathematically be expressed as [5]

$$g\left(\hat{t}\right)=\sin\left(\frac{\pi\hat{t}}{\hat{T}}\right)U\left(\hat{t}\right)+\sin\left(\frac{\pi}{\hat{T}}\left(\hat{t}-\hat{T}\right)\right)U\left(\hat{t}-\hat{T}\right) \tag{8}$$

where $\hat{T}$ is the shock duration and U is the unit step function.

Introducing the dimensionless variables $u=\frac{a\hat{u}}{d^2}$, $v=\frac{b\hat{v}}{d^2}$, $w=\frac{\hat{w}}{d}$, $x=\frac{\hat{x}}{a}$, $y=\frac{\hat{y}}{b}$ and $t=\hat{t}/t_0$, the non-dimensional form of the governing equations of motion in (3) is obtained as

$$u_{,xx}+w_{,x}w_{,xx}+\frac{\alpha_1^2(1-\nu)}{2}\left(u_{,yy}+w_{,x}w_{,yy}\right)+\frac{\alpha_1^2(1+\nu)}{2}\left(v_{,xy}+w_{y}w_{,xy}\right)=0 \tag{9a}$$

$$\alpha_1^4\left(v_{,yy}+w_{,y}w_{,yy}\right)+\frac{\alpha_1^2(1-\nu)}{2}\left(v_{,xx}+w_{,y}w_{,xx}\right)+\frac{\alpha_1^2(1+\nu)}{2}\left(u_{,xy}+w_{x}w_{,xy}\right)=0 \tag{9b}$$

$$\left(\frac{1}{12}\right)\left(w_{,xxxx}+2\alpha_1^2 w_{,xxyy}+\alpha_1^4 w_{,yyyy}\right)+w_{,tt}$$
$$=\frac{\beta}{(1-w)^2}+\alpha_2^2\Big\{w_{,xx}\Big[u_{,x}+\frac{1}{2}w_{,x}^2+\nu\alpha_1^2$$
$$\times\left(v_{,y}+\frac{1}{2}w_{,y}^2\right)\Big]+w_{,xy}\left[(1-\nu)\alpha_1^2\left(u_{,y}+v_{,x}+w_{,x}w_{,y}\right)\right]+w_{,yy}\Big[\alpha_1^4\left(v_{,y}+\frac{1}{2}w_{,y}^2\right)$$
$$+\nu\left(u_{,x}+\frac{1}{2}w_{,x}^2\right)\Big]\Big\}+\lambda\bar{g}(t) \tag{9c}$$

where α_i $(i=1,2)$, β and λ are the normalized parameters of the problem and, respectively, are named as the micro-plate aspect ratio as well as the gap, electrostatic and shock amplitude parameters. These parameters are given by

$$\alpha_1=\frac{a}{b},\quad \alpha_2=\frac{d}{h},\quad \beta=\frac{\varepsilon a^4\left(1-\nu^2\right)V^2}{2Eh^3d^3},\quad \lambda=\frac{\rho a_0 a^4\left(1-\nu^2\right)}{Eh^2d} \tag{10}$$

Also, the time scale t_0, which is determined such that the coefficient of $w_{,tt}$ becomes unity, is defined as

$$t_0=\sqrt{\frac{\rho a^4\left(1-\nu^2\right)}{Eh^2}} \tag{11}$$

Furthermore, the dimensionless shock profile $\bar{g}(t)$ is determined as

$$\bar{g}(t)=\sin\left(\frac{\pi t}{T}\right)U(t)+\sin\left(\frac{\pi}{T}(t-T)\right)U(t-T) \tag{12}$$

It is noted that, t in Eqs. (9c) and (12) is dimensionless time and T is dimensionless shock duration expressed by

$$T=\frac{\hat{T}}{t_0} \tag{13}$$

Here, zero initial conditions as well as fully clamped with immovable edges boundary conditions for the present systems are assumed. Hence, the non-dimensional form of the boundary conditions takes the form

$$u=v=w=w_{,x}=w_{,y}=0 \quad \text{at} \quad x=0,\ 1 \tag{14a}$$

$$u=v=w=w_{,x}=w_{,y}=0 \quad \text{at} \quad y=0,\ 1 \tag{14b}$$

3 Solution Methodology

As it is mentioned in the Sect. 1, generating ROMs for analyzing MEMS applications especially those subjected to mechanical shock represents many desirable features. According to the general basis of the reduced order modeling procedure, the governing PDEs of motion should be discretized to a finite degree-of-freedom system consisting of ODEs in time employing some typical mathematical techniques such as the GWRM [17, 45]. It is worth noting that utilizing the available ROMs in the literature for rectangular micro-plates, which pre-multiplies the transverse governing equation of motion by the denominator of the electrostatic forcing term, leads to a complex system of ODEs in time [16, 17]. Because, this pre-multiplication, avoiding from which has seriously been suggested by Askari and Tahani [5], adds the significant effects of higher-order modes and leads to the requirement of utilizing a computationally very expensive multi-mode reduced order modelling [5, 46]. Hence, employing these ROMs for analyzing dynamics of MEMS structures under shock acceleration, whose behaviors are much more non-linear than those not subjected to the mechanical shock [6, 7], is not appropriate at all. Therefore, in view of our previous ROM presented for beam-type MEMS [5], an alternative single DOF model will be developed in the present paper for rectangular micro-plates subjected to the combined actions of electrostatic attraction and shock pulse acceleration.

To generate the present ROM, at the first step, the in-plane displacements u and v are approximated in terms of the out-of-plane deflection w by applying the GWRM on linear Eqs. (9a) and (9b). For this purpose, since it is proved that utilizing only one basis function for approximating the transverse deflection can accurately predict the pull-in instability threshold [5, 39], the displacement filed are discretized as

$$u(x,y,t) = w_0^2(t) \sum_{i=1}^{n} \sum_{j=1}^{n} u_{ij} \varphi_u^{ij}(x,y) \tag{15a}$$

$$v(x,y,t) = w_0^2(t) \sum_{i=1}^{n} \sum_{j=1}^{n} v_{ij} \varphi_v^{ij}(x,y) \tag{15b}$$

$$w(x,y,t) = w_0(t) \varphi_w(x,y) \tag{15c}$$

where w_0, u_{ij} and v_{ij} are some unknowns which should be determined. Also, the admissible basis functions $\varphi_u^{ij}(x,y)$, $\varphi_v^{ij}(x,y)$ and $\varphi_w(x,y)$, which must identically satisfy all boundary conditions presented in Eq. (14), are selected as [41, 47]

$$\varphi_u^{ij}(x,y) = \sin(i\pi x)\sin(j\pi y) \tag{16a}$$

$$\varphi_v^{ij}(x,y) = \sin(i\pi x)\sin(j\pi y) \tag{16b}$$

$$\varphi_w(x,y) = \psi(x)\psi(y) \tag{16c}$$

in which ψ is the first eigen-mode of an undeformed doubly clamped beam given by [5]

$$\psi(\xi) = \cosh(\gamma\xi) - \cos(\gamma\xi) - \vartheta[\sinh(\gamma\xi) - \sin(\gamma\xi)] \tag{17}$$

where

$$\gamma = 4.7300, \quad \vartheta = 0.9825 \tag{18}$$

It is to be noted that substituting the displacement field from Eq. (15) into Eqs. (9a) and (9b), and then simplifying w_0^2 from both sides of these equations, the values of u_{ij} and v_{ij} will be obtained through employing the GWRM. To complete the solution methodology and generate the present ROM, it is sufficient to find the generalized coordinate w_0. For this object, one should substitute from Eq. (15) into Eq. (9c), multiply both sides of this equation by $\varphi_w(x, y)$ and integrate the outcome over the whole dimensionless region. Hence, the present ROM is generated as

$$\ddot{w}_0 + \mathcal{K}_1 w_0 + \mathcal{K}_2 w_0^3 = \mathcal{K}_3 \bar{g}(t) + \beta \int_0^1 \int_0^1 \frac{\varphi_w}{\left(1 - \varphi_w w_0\right)^2} \, dxdy \tag{19}$$

where dot-superscript denotes the differentiation with respect to the dimensionless time variable t and the coefficients $\mathcal{K}_1$, $\mathcal{K}_2$ and $\mathcal{K}_3$ are defined as

$$\mathcal{K}_1 = \frac{1}{12} \int_0^1 \int_0^1 \left(\varphi_{w,xxxx} + 2\alpha_1^2 \varphi_{w,xxyy} + \alpha_1^4 \varphi_{w,yyyy}\right) \varphi_w dxdy \tag{20a}$$

$$\begin{aligned}\mathcal{K}_2 = -\alpha_2^2 \int_0^1 \int_0^1 \Bigg\{ & \varphi_{w,xx} \left[\sum_{i=1}^{n} \sum_{j=1}^{n} u_{ij} \varphi_{u,x}^{ij} + \frac{1}{2} \varphi_{w,x}^2 + \nu\alpha_1^2 \left(\sum_{i=1}^{n} \sum_{j=1}^{n} v_{ij} \varphi_{v,y}^{ij} + \frac{1}{2} \varphi_{w,y}^2 \right) \right] \\ & + \varphi_{w,yy} \left[\alpha_1^4 \left(\sum_{i=1}^{n} \sum_{j=1}^{n} v_{ij} \varphi_{v,y}^{ij} + \frac{1}{2} \varphi_{w,y}^2 \right) + \nu \left(\sum_{i=1}^{n} \sum_{j=1}^{n} u_{ij} \varphi_{u,x}^{ij} + \frac{1}{2} \varphi_{w,x}^2 \right) \right] \\ & + (1-\nu)\alpha_1^2 \varphi_{w,xy} \left(\sum_{i=1}^{n} \sum_{j=1}^{n} u_{ij} \varphi_{u,y}^{ij} + \sum_{i=1}^{n} \sum_{j=1}^{n} v_{ij} \varphi_{v,x}^{ij} + \varphi_{w,x} \varphi_{w,y} \right) \Bigg\} \varphi_w \, dxdy \end{aligned} \tag{20b}$$

$$\mathcal{K}_3 = \lambda \int_0^1 \int_0^1 \varphi_w dxdy \tag{20c}$$

As it is seen from Eq. (19), employing the present ROM reduces the governing nonlinear system of PDEs of motion to a single initial value problem (IVP). Therefore, the motion of the micro-plate will simply be simulated through the solution of the IVP presented in Eq. (19) with its zero initial conditions. This fact significantly reduces the

run-time of the problem which provides us to investigate the response of the system under mechanical shock.

In the present study, the reduced governing equation of motion (i.e. Eq. (19)) will be solved using the fourth order Runge–Kutta method [48]. Furthermore, for the purpose of validation, the static configuration of the present system will also be obtained by applying the Newton–Raphson procedure [48] on the ROM presented in Eq. (19) without its inertia term. It is worth mentioning that the values of the stiffness coefficients $\mathcal{K}_1$ and $\mathcal{K}_2$ only depend on the micro-plate aspect ratio and the gap parameter. Therefore, one can significantly decrease the time which requires for finding the instability threshold of the system through computing and saving the values of these coefficients and calling them during the solution procedure of the reduced equation.

4 Results and Discussions

To verify the accuracy of the findings, besides comparison to available static results in the literature, 3-D FE simulations are also utilized in the present paper. To this end, a square silicon micro-plate with fully clamped boundary conditions as well as geometric and material properties given in Table 1 is considered. Furthermore, 3-D brick elements together with the physics of *Electromechanics*, which is suitable for systems governed by the coupled structural and electrical physics, are employed to model the micro-plate in COMSOL Multiphysics commercial software [42]. It is to be noted that the dimensions of the present system have been selected such that they match with the case statically analyzed by Zhao et al. [16] and take place in the range of typical microstructures dimensions [5–7].

To find the required number of in-plane modes in each direction (i.e. n), which should be included into the present ROM, Fig. 2 represents a convergence study on the micro-plate mid-point deflection versus the values of the dimensionless input voltage. In addition, this figure provides a comparison between the converged static findings obtained by the present ROM and those calculated through the 3-D FE simulation carried out in COMSOL Multiphysics [42], as well as the results reported by Zhao et al. [16]. It is to be mentioned here that the electrostatic parameters reported by Zhao et al. [16] are pre-multiplied by the coefficient of $1/12$; because their non-dimensionalization procedure differs from the present one.

As it can be observed from Fig. 2, the present ROM converges when the number of in-plane modes in each direction is set to $n=4$. Also, according to this figure, the present ROM and FE findings agree excellently with each other as well as those reported by Zhao et al. [16].

It is to be noted that the results of the present single DOF model are so accurate in comparison to multi-mode observations reported by Zhao et al. [16]. The reason for

Table 1 Geometric and material properties of a square micro-plate made of silicon [52]

a (μm)	h (μm)	d (μm)	E (GPa)	ν	ρ (kg/m^3)
1000	1.5	1.5	169	0.3	2332

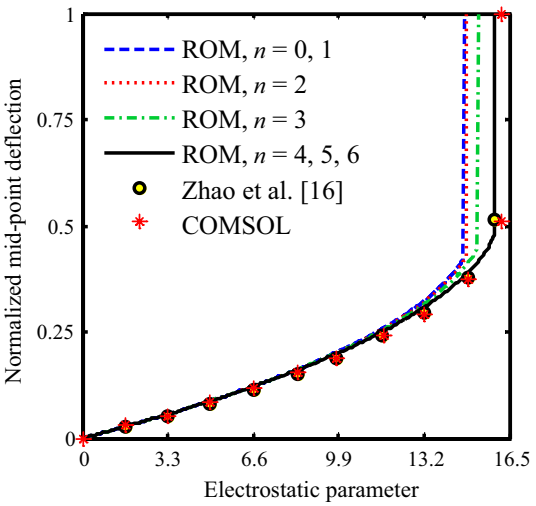

Fig. 2 Comparison between the static configurations obtained by different methods for a system with normalized properties $\alpha_1 = \alpha_2 = 1$ and $\nu = 0.3$

this fact is that the deformed configuration of the micro-plate under the combined action of the electrostatic excitation and shock pulse acceleration is very similar to its first natural mode. In this way, it is worth mentioning that since Zhao et al. [16] pre-multiplied the transverse governing equation of motion by the denominator of the electrostatic forcing term, the weighting functions of their GWRM were changed which results in the change of its convergence speed [46, 49]. Therefore, they were forced to employ higher transverse natural modes for generating a convergent ROM with accurate results.

To validate the accuracy of the present findings for cases subjected to the mechanical shock, a square silicon micro-plate with properties given in Table 1 is considered again. It is to be mentioned here that the duration of the shock pulse is so important and plays a crucial role in the response of the micro-structure. Micro-structures can experience two different types of loadings under the application of the mechanical shock: quasi-static loading and dynamic one [5, 7]. Quasi-static loading, in which the response of the structure resembles to the shock profile, occurs when the shock duration is far from the first natural period of the structure [5, 7]. However, due to the resonance-like behavior of the system, the dynamic loading is observed when the duration of the shock acceleration closes to the first natural period of the structure [5, 7]. According to JEDEC regulations [50], the duration of shock accelerations can vary from 0.1 to 1 ms which covers all possible cases for the hard-floor drop test. Therefore, since the first natural period of the present micro-plate can simply be calculated as $\tau = 0.045$ ms [51], the quasi-static and dynamic responses will be observed, for the shock durations $\hat{T} = 1$ ms and $\hat{T} = 0.1$ ms, respectively.

Table 2 investigates the convergence of dynamic pull–in voltages for the present square silicon micro-plate with properties presented in Table 1. This micro-plate is subjected to shock pulse accelerations with the amplitude of 1500 g and durations $\hat{T} = 1$ ms (quasi-static loading case) and $\hat{T} = 0.1$ ms (dynamic loading case). It is to be mentioned here that such a large value for the shock pulse amplitude is selected in

Table 2 Convergence of dynamic pull–in voltages (V) in both quasi-static and dynamic loading cases for a square micro-plate under the action of shock acceleration with the amplitude of 1500 g and properties given in Table 1

Method	Quasi-static loading case	Dynamic loading case
ROM ($n=0$)	0.67	0.51
ROM ($n=1$)	0.67	0.51
ROM ($n=2$)	0.70	0.56
ROM ($n=3$)	0.83	0.71
ROM ($n=4$)	0.98	0.90
ROM ($n=5$)	0.98	0.90
ROM ($n=6$)	0.98	0.90
FE simulation (COMSOL)	1.04	0.95

Table 2 to ensure the convergence of the present approach in all possible cases even for the ones subjected to enormous shock accelerations. According to this table, the present approach in both quasi-static and dynamic cases converges when the number of in-plane modes in each direction is set to $n=4$. Therefore, hereinafter the results of the present study are calculated using $n=4$.

To verify the accuracy of the converged values of dynamic pull–in voltages in both quasi-static and dynamic loading cases, a 3-D FE simulation in COMSOL Multiphysics [42] is also performed. It is to be mentioned here that the aforementioned FE model together with the time-dependent study is employed for the dynamic analysis where the shock is applied to the micro-plate as a distributed load per unit area. Employing the FE model, the values of dynamic pull–in voltages for the present micro-plate with properties presented in Table 1 under the same loading conditions are calculated. According to Table 2, the converged values of dynamic pull–in voltages, in both quasi-static and dynamic loading cases, agree excellently with those obtained by 3-D FE simulation.

As it can be observed from Table 2, in-plane displacements play a crucial role in the instability threshold of electrically actuated micro-plates. It is worth noting that although neglecting the in-plane displacements reduces the system of governing PDEs of motion to a single one and significantly simplifies the solution procedure of the problem, it may generate enormous errors which cannot be ignored. According to Table 2, this simplification produces the significant errors of 31.63 and 43.33% for quasi-static and dynamic loading cases, respectively. However, as it can be observed from Fig. 2, neglecting the in-plane displacements makes the error of only 4% in the calculation of the static pull–in voltage of the system. Hence, it can be concluded that the in-plane displacements play a much more crucial role in the dynamic instability threshold of the system than its static one. Therefore, it is so essential to account for the influence of in-plane displacements for systems under mechanical shock especially those subjected to dynamic loading conditions.

Based on the results presented in Fig. 2 and Table 2, there exist no differences between the case in which the in-plane displacements have been neglected and the one in which they have been calculated using single mode approximation. To investigate this issue more, the values of u_{ij} and v_{ij} have been presented in Table 3 for a

system with the same properties when the number of in-plane modes in each direction is set to $n=4$. It is to be noted that, according to Eqs. (9) and (15), the values of u_{ij} and v_{ij} are independent from the type of loading as well as the value of input voltage, and only depend on the Poisson and aspect ratios of the system. Based on the results written in this table, u_{ij} for the odd values of i and the even values of $-j$ becomes zero. Also v_{ij} vanishes when the indices i and j, respectively, take the even and odd values. This is due to the symmetry of the system which forces the in-plane displacements u and v to vanish on the center-lines $x = 0.5$ and $y = 0.5$, respectively. In addition, this symmetry causes the in-plane displacements u and v to take their maximum values on the center-lines $y = 0.5$ and $x = 0.5$, respectively. Hence, the values of u_{ij} and v_{ij}, which are incompatible with these symmetric conditions, become zero. This is the reason of the fact that approximating the in-plane displacements using only one basis functions cannot improve the findings of the present ROM; because both u_{11} and v_{11} are zero.

It is worth mentioning that using this important feature of the present ROM, which is only due to the symmetry of the present system and cannot be applied to an asymmetric problem, the basis functions $\varphi_u^{ij}(x, y)$ and $\varphi_v^{ij}(x, y)$ can modify to

$$\varphi_u^{ij}(x, y) = \sin(2i\pi x) \sin\left[(2j-1)\pi y\right] \tag{21a}$$

$$\varphi_v^{ij}(x, y) = \sin\left[(2i-1)\pi x\right] \sin(2j\pi y) \tag{21b}$$

It is to be noted that by applying the aforementioned modification, the number of required in-plane modes in each direction for the modified version of the present ROM is reduced to $n = 2$. Hence, since this technique significantly decreases the computations and so the run-time of the present problem, hereinafter, it will be applied on the present ROM for obtaining further results.

To investigate the response of the present system to both quasi-static and dynamic loadings more, the micro-plate with properties similar to those presented in Table 1 is considered again. Employing the present ROM, the dynamic pull–in voltage for this micro-plate without considering the effect of shock acceleration is determined as $V_{\mathrm{DPI}} = 2.52$ V which matches exactly with the value obtained by 3-D FE simulation. Figure 3a and b depict time histories of both stable and unstable mid-point deflections for this system under the action of shock pulse acceleration with the amplitude of 1500 g and durations $\hat{T} = 1$ ms (quasi-static loading case) and $\hat{T} = 0.1$ ms (dynamic loading case), respectively. According to Fig. 3, it is obvious that besides the intensity of the electrostatic field, the instability threshold of the

Table 3 Values of u_{ij} and v_{ij} for a square micro-plate with properties presented in Table 1

	u_{ij}				v_{ij}			
	$j=1$	$j=2$	$j=3$	$j=4$	$j=1$	$j=2$	$j=3$	$j=4$
$i=1$	0.00	0.00	0.00	0.00	0.00	−0.07	0.00	0.76
$i=2$	−0.07	0.00	0.57	0.00	0.00	0.00	0.00	0.00
$i=3$	0.00	0.00	0.00	0.00	0.00	0.57	0.00	−0.30
$i=4$	0.76	0.00	−0.30	0.00	0.00	0.00	0.00	0.00

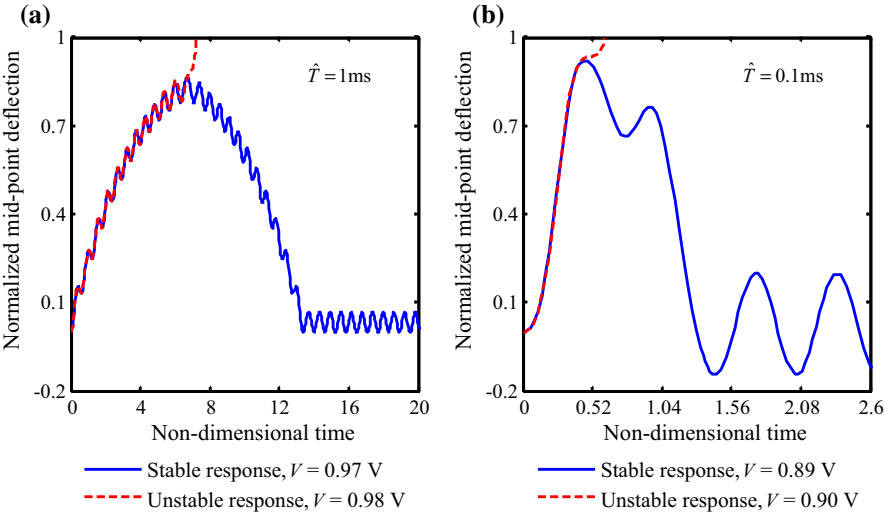

Fig. 3 Time-histories of mid-point deflection for a square silicon micro-plate with properties presented in Table 1, when it is subjected to the shock pulse acceleration with the amplitude of 1500 g; **a** quasi-static and **b** dynamic loading conditions

system is significantly affected by the shock pulse acceleration as well as the type of the loading. Furthermore, based on the results shown in this figure, the unstable pull–in behavior in dynamic loading conditions occurs at voltages less than those in quasi-static one. Because, due to the resonance-like behavior of the structure, dynamic loading vibrates the micro-plate with the amplitude more than that happens under quasi-static loading. This increase of the micro-plate deflection significantly increases the effect of electrostatic attraction which results in the reduction of the dynamic pull–in voltage in this case.

As it is mentioned above, dynamic instability threshold of the system is significantly affected by the shock amplitude and the loading type. To illustrate this issue more, Fig. 4a and b, respectively, depict the variation of dynamic pull–in voltages versus the values of shock amplitudes for the present micro-plate under quasi-static ($\hat{T} = 1$ ms) and dynamic ($\hat{T} = 0.1$ ms) loadings. These figures also represent a comparison between present findings and those obtained by 3-D FE simulation. According to Fig. 4, the present ROM results agree excellently with FE findings in both quasi-static and dynamic loading cases.

As it is seen from Fig. 4, increasing the values of shock amplitudes significantly reduces the dynamic instability threshold of the system especially when it is subjected to dynamic loading conditions. Therefore, it is so important to account for the interaction between electrostatic attraction and shock pulse acceleration in designing micro-devices to prevent them from undesirable dynamic pull–in instabilities under environmental forces even for the ones which operate within the small range of input voltage. In addition, as it is mentioned in the Sect. 1, dynamic pull–in under the combined actions of electrostatic attraction and mechanical shock is not undesirable in all cases. This phenomenon may be desirable and considered as the basis of the

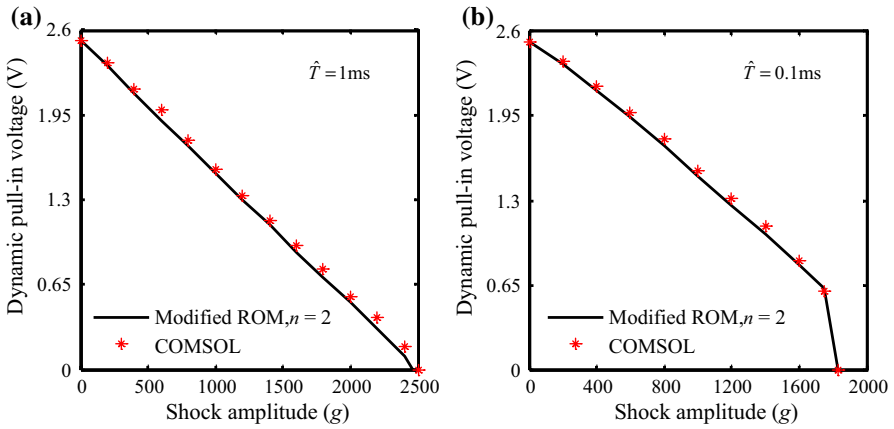

Fig. 4 Dynamic pull–in voltages (V) versus shock amplitudes (g) for the present micro-plate with properties given in Table 1; **a** quasi-static and **b** dynamic loading cases

sensing method in some cases such as sensors of vehicles airbags [5]. Therefore, regardless the type and the application of a micro-device, it is so essential to determine its instability threshold under mechanical shock accurately.

To find the instability threshold of a system under a certain value of shock amplitude, it needs to simulate the motion of the system for some different values of input voltages. This procedure takes only a few minutes when the present ROM is utilized. However, employing the present FE model, it sometimes lasts several hours especially for cases under enormous shock accelerations. It is to be mentioned here that although the so long run-time limitation of the FE procedure for beam-type MEMS has successfully been removed in our previous paper [5], there exists no alternative method for the analysis of electrically actuated micro-plates in the literature. Therefore, due to the accuracy, robustness and very short run-time of the present approach, it can be considered as an alternative and promising tool for simulating and designing plate-type MEMS especially those subjected to mechanical shock.

5 Conclusions

The present paper focused on the dynamic pull–in instability of rectangular plate-type MEMS under mechanical shock. For this object, a novel and computationally very efficient ROM was employed which could reduce the system of governing PDEs of motion to an ODE in time. The present ROM was also improved for systems with symmetric boundary conditions and its convergence speed in such systems was accelerated. Using the present fast convergent solution procedure, the motion of a micro-plate with fully clamped boundary conditions was analyzed and its dynamic instability threshold under mechanical shock was studied. It was found that an electrically actuated micro-plate may pull–in under an external voltage much less than its dynamic pull–in voltage if it is subjected to mechanical shock. Furthermore, due

to the resonance-like behavior of the structure, if the shock duration closes to the first natural period of the structure, this reduction of the dynamic instability threshold will be more highlighted. The accuracy of the present approach was also verified through direct comparison between its static results and those published in the literature. In addition, due to the lack of reports in the literature for dynamic pull–in voltages of systems subjected to mechanical shock, the present findings were compared and validated by those obtained through 3-D FE simulation performed in COMSOL Multiphysics commercial software. It was found that the present ROM can successfully remove the long run-time limitation of the FE simulation and produce accurate and robust results over the whole operation range of the system.

References

1. Senturia, S. D. (2001). *Microsystem design*. Dordrecht: Kluwer Academic Publishers.
2. Batra, R. C., Porfiri, M., & Spinello, D. (2007). Review of modeling electrostatically actuated microelectromechanical systems. *Smart Materials and Structures, 16,* 23–31.
3. Nayfeh, A. H., & Younis, M. I. (2005). Dynamics of MEMS resonators under superharmonic and subharmonic excitations. *Journal of Micromechanics and Microengineering, 15,* 1840–1847.
4. Rebeiz, G. M. (2003). *RF MEMS: Theory, design, and technology*. NewYork: Wiley.
5. Askari, A. R., & Tahani, M. (2014). An alternative reduced order model for electrically actuated micro-beams under mechanical shock. *Mechanics Research Communications, 57,* 34–39.
6. Younis, M. I., Miles, R., & Jordy, D. (2006). Investigation of the response of microstructures under the combined effect of mechanical shock and electrostatic forces. *Journal of Micromechanics and Microengineering, 16,* 2463–2474.
7. Younis, M. I., Alsaleem, F., & Jordy, D. (2007). The response of clamped–clamped microbeams under mechanical shock. *International Journal of Non-Linear Mechanics, 42,* 643–657.
8. Béliveau, A., Spencer, G. T., Thomas, K. A., & Roberson, S. L. (1999). Evaluation of MEMS capacitive accelerometers. *IEEE Design & Test of Computers, 16,* 48–56.
9. Brown, T. G., Davis, B., Hepner, D., Faust, J., Myers, C., Muller, P., et al. (2001). Strapdown microelectromechanical (MEMS) sensors for high-G munition applications. *IEEE Transactions on Magnetics, 37,* 336–342.
10. Fan, M. S., & Shaw, H. C. (2001). Dynamic response assessment for the MEMS accelerometer under severe shock loads. In *Proceedings of NASA*, TP-2001-20997.
11. Fang, X. W., Huang, Q. A., & Tang, J. Y. (2004). Modeling of MEMS reliability in shock environments. In *Proceedings of 7th international conference on solid-state and integrated circuits technology* (pp. 860–863).
12. Younis, M. I. (2011). *MEMS linear and nonlinear statics and dynamics*. New York: Springer.
13. Krylov, S. (2007). Lyapunov exponents as a criterion for the dynamic pull-in instability of electrostatically actuated microstructures. *International Journal of Non-Linear Mechanics, 42,* 626–642.
14. Abdel-Rahman, E. M., Younis, M. I., & Nayfeh, A. H. (2002). Characterization of the mechanical behavior of an electrically actuated microbeam. *Journal of Micromechanics and Microengineering, 12*(6), 759–766.
15. Younis, M. I., Abdel-Rahman, E. M., & Nayfeh, A. H. (2003). A reduced-order model for electrically actuated microbeam based MEMS. *Journal of Microelectromechanical systems, 12,* 672–680.
16. Zhao, X., Abdel-Rahman, E. M., & Nayfeh, A. H. (2004). A reduced-order model for electrically actuated microplates. *Journal of Micromechanics and Microengineering, 14,* 900–906.
17. Nayfeh, A. H., Younis, M. I., & Abdel-Rahman, E. M. (2005). Reduced-order models for MEMS applications. *Nonlinear Dynamics, 41*(1), 211–236.
18. Kuang, J.-H., & Chen, C.-J. (2004). Dynamic characteristics of shaped micro-actuators solved using the differential quadrature method. *Journal of Micromechanics and Microengineering, 14*(4), 647.
19. Sadeghian, H., Rezazadeh, G., & Osterberg, P. M. (2007). Application of the generalized differential quadrature method to the study of pull–in phenomena of MEMS switches. *Journal of Microelectromechanical Systems, 16*(6), 1334–1340.

20. Jin, C., Jiang, Z., & Xingtao, W. (2004). Analytical and finite element model pull–in study of rigid and deformable electrostatic microactuators. *Journal of Micromechanics and Microengineering, 14*(1), 57.
21. Moghimi Zand, M., & Ahmadian, M. T. (2010). Dynamic pull–in instability of electrostatically actuated beams incorporating Casimir and van der Waals forces. *Journal of Mechanical Engineering Science, 224*(9), 2037–2047.
22. Tajalli, S. A., Moghimi Zand, M., & Ahmadian, M. T. (2009). Effect of geometric nonlinearity on dynamic pull-in behavior of coupled-domain microstructures based on classical and shear deformation plate theories. *European Journal of Mechanics-A/Solids, 28*(5), 916–925.
23. Hung, E. S., & Senturia, S. D. (1999). Generating efficient dynamical models for microelectromechanical systems from a few finite-element simulation runs. *Journal of Microelectromechanical Systems, 8*(3), 280–289.
24. Mohsenzadeh, A., Tahani, M., & Askari, A. R. (2015). A Novel Method for Investigating the Casimir effect on pull–in instability of electrostatically actuated fully clamped rectangular nano/microplates. *Journal of Nanoscience, 2015,* 9.
25. Tahani, M., Askari, A. R., Mohandes, Y., & Hassani, B. (2015). Size-dependent free vibration analysis of electrostatically pre-deformed rectangular micro-plates based on the modified couple stress theory. *International Journal of Mechanical Sciences, 94–95,* 185–198.
26. Tahani, M., & Askari, A. R. (2014). Accurate electrostatic and van der Waals pull–in prediction for fully clamped nano/micro-beams using linear universal graphs of pull–in instability. *Physica E: Low-dimensional Systems and Nanostructures, 63,* 151–159.
27. Askari, A. R., & Tahani, M. (2012). Analytical approximations to nonlinear vibration of a clamped nanobeam in presence of the Casimir force. *International Journal of Aerospace and Lightweight Structures, 2*(3), 317–334.
28. Askari, A. R., & Tahani, M. (2012). Investigating nonlinear vibration of a fully clamped nanobeam in presence of the van der Waals attraction. *Applied Mechanics and Materials, 226–228,* 181–185.
29. Askari, A. R., & Tahani, M. (2016). Stability analysis of electrostatically actuated nano/microbeams under the effect of van der Waals force, a semi-analytical approach. *Communications in Nonlinear Science and Numerical Simulation, 34,* 130–141.
30. Koochi, A., Sedighi, H. M., & Abadyan, M. (2014). Modeling the size dependent pull–in instability of beam-type NEMS using strain gradient theory. *Latin American Journal of Solids and Structures, 11,* 1806–1829.
31. Dashtaki, P. M., & Beni, Y. T. (2014). Effects of Casimir force and thermal stresses on the buckling of electrostatic nanobridges based on couple stress theory. *Arabian Journal for Science and Engineering, 39*(7), 5753–5763.
32. Beni, Y. T., Koochi, A., & Abadyan, M. (2014). Using modified couple stress theory for modeling the size dependent pull-in instability of torsional nano-mirror under Casimir force. *International Journal of Optomechatronics, 8,* 47–71.
33. Tadi Beni, Y., Karimipour, I., & Abadyan, M. (2015). Modeling the instability of electrostatic nanobridges and nano-cantilevers using modified strain gradient theory. *Applied Mathematical Modelling, 39*(9), 2633–2648.
34. Sedighi, H. M., Daneshmand, F., & Abadyan, M. (2015). Modified model for instability analysis of symmetric FGM double-sided nano-bridge: Corrections due to surface layer, finite conductivity and size effect. *Composite Structures, 132,* 545–557.
35. Malihi, S., Beni, Y. T., & Golestanian, H. (2016). Analytical modeling of dynamic pull-in instability behavior of torsional nano/micromirrors under the effect of Casimir force. *Optik, 127*(10), 4426–4437.
36. Milad, S., Yaghoub Tadi, B., & Hossein, A. (2016). Size-dependent snap-through and pull-in instabilities of initially curved pre-stressed electrostatic nano-bridges. *Journal of Physics D: Applied Physics, 49*(29), 295303.
37. Malihi, S., Tadi Beni, Y., & Golestanian, H. (2016). Size dependent pull–in instability analysis of torsional nano/micromirrors in the presence of molecular force using 2D model. *Optik, 127*(19), 7520–7536.
38. Malihi, S., Beni, Y. T., & Golestanian, H. (2017). Dynamic pull–in stability of torsional nano/micromirrors with size-dependency, squeeze film damping and van der Waals effect. *Optik, 128,* 156–171.
39. Askari, A. R., & Tahani, M. (2017). Size-dependent dynamic pull-in analysis of geometric nonlinear micro-plates based on the modified couple stress theory. *Physica E: Low-dimensional Systems and Nanostructures, 86,* 262–274.

40. Français, O., & Dufour, I. (1999). Normalized abacus for the global behavior of diaphragms: Pneumatic, electrostatic, piezoelectric or electromagnetic actuation. *Journal of Modeling and Simulation of Microsystems, 1*(2), 149–160.
41. Batra, R. C., Porfiri, M., & Spinello, D. (2008). Reduced-order models for microelectromechanical rectangular and circular plates incorporating the Casimir force. *International Journal of Solids and Structures, 45,* 3558–3583.
42. COMSOL Multiphysics, Version 5.2a, Burlington, MA 01803 (2016). http://www.comsol.com. Accessed Jan 2018.
43. Reddy, J. N. (2007). *Theory and analysis of elastic plates and shells* (2nd ed.). Philadelphia: Taylor & Francis.
44. Yeh, C.-L., & Lai, Y.-S. (2006). Support excitation scheme for transient analysis of JEDEC board-level drop test. *Microelectronics Reliability, 46*(2–4), 626–636.
45. Reddy, J. N. (2002). *Energy principles and variational methods in applied mechanics*. New York: Wiley.
46. Gutschmidt, S. (2010). The influence of higher-order mode shapes for reduced-order models of electrostatically actuated microbeams. *Journal of Applied Mechanics, 77*(4), 0410071–0410076.
47. Amabili, M. (2004). Nonlinear vibrations of rectangular plates with different boundary conditions: theory and experiments. *Computers & Structures, 82*(31–32), 2587–2605.
48. Faires, J. D., & Burden, R. L. (2002). *Numerical methods* (3rd ed.). Pacific Grove: Brooks/Cole.
49. Askari, A. R. (2018). The influence of higher in- and out-of-plane natural modes on dynamic pull-in instability of electrically actuated micro-plates. *European Journal of Computational Mechanics*. https://doi.org/10.1080/17797179.2018.1484032. **(In Press)**.
50. JEDEC Solid State Technology Association. (2001). *JESD22-B110: Subassembly Mechanical Shock*. VA: Arlington.
51. Arenas, J. P. (2003). On the vibration analysis of rectangular clamped plates using the virtual work principle. *Journal of Sound and Vibration, 266,* 912–918.
52. Osterberg, P. M. (1995). *Electrostatically actuated microelectromechanical test structures for material property measurement*. Cambridge: Massachusetts Institute of Technology.